On the Correlated *k*-Distribution Method for Radiative Transfer in Nonhomogeneous Atmospheres

QIANG FU AND K. N. LIOU

Department of Meteorology/CARSS, University of Utah, Salt Lake City, Utah

(Manuscript received 3 December 1991, in final form 15 April 1992)

ABSTRACT

The correlated *k*-distribution method for radiative transfer in nonhomogeneous atmospheres is discussed in terms of the physical and mathematical conditions under which this method is valid. Two correlated conditions are necessary and sufficient for the exact transformation of the wavenumber integration to an integration over the cumulative probability (g), a monotonically increasing and smooth function in the absorption coefficient space. These conditions involve the use of a reference condition to define the absorption coefficient and an assumption concerning the ordering of the absorption coefficient. The correlated conditions are exact in the context of a single line, periodic lines, and the strong- and weak-line limits. In realistic atmospheres, these assumptions are best for adjacent levels but produce increasing blurring or deviations for distant levels.

We investigate the blurring of the correlated assumptions on the computations of fluxes and heating rates based on "exact" line-by-line results, using a variety of atmospheric profiles and spectral intervals containing principal absorbing gases. In the thermal infrared, errors in fluxes are less than 0.2% for H_2O, CO_2, CH_4, and N_2O, and ~2% for O_3. Errors in heating rates are less than 0.01 K day^{-1} for these gases below ~30 km. Larger errors of ~0.1 K day^{-1} can occur at some levels above this height. For H_2O lines in the solar region, errors in fluxes and heating rates are within 0.05% and 0.01 K day^{-1}, respectively. Based on numerical experimentation, we find that the number of g values ranging from 1 (for weak bands) to ~10 (for strong bands) are usually sufficient to achieve acceptable accuracy for flux and heating rate calculations.

The correlated *k*-distribution method differs fundamentally from the traditional approach that employs scaling approximations and band models to separate height and wavenumber integrations for transmittance calculations. The equivalent k values for various gases computed from this approach can be directly incorporated in the multiple-scattering program involving cloud and aerosol particles.

1. Introduction

The radiative transfer process is essentially the process of interactions between matter and a radiation field. These interactions may be classified as absorption, scattering, or emission, all of which can be described by the equation of radiative transfer (Liou 1980; Goody and Yung 1989). Because the radiative processes that we normally consider are frequency coherent, the independent variable that is physically appropriate for such processes is the wavenumber (or wavelength). Thus, the solutions involving multiple-scattering processes are dependent on the wavenumber (see, e.g., Liou et al. 1988). For a given spectral interval, these solutions must be integrated in the wavenumber domain. However, because of the nongray nature of atmospheric absorption due to a large number of spectral lines produced by the radiatively active gases, the integration requires very small wavenumber increments. Enormous computer time is needed to achieve desirable accuracy. Consequently, there is a practical need to parameterize the nongray gaseous absorption in a form that is suitable for treating the multiple-scattering problem. This is particularly important in view of the fact that clouds are the main modulator of the radiation field in planetary atmospheres.

As discussed by Stephens (1984), the use of the so-called k(absorption coefficient)-distribution method (Arking and Grossman 1972; Domoto 1974; Chou and Arking 1980) would appear to be a useful approach for the computation of infrared radiative transfer. This method was originally proposed by Ambartzumian (1936) in the work on stellar atmospheres. For a homogeneous atmosphere, the transmittance within a spectral interval is independent of the ordering of the value of k with respect to wavenumber, but depends only on the fraction of the interval that is associated with a particular value of k. A major advantage of the *k*-distribution method is that it can be readily incorporated into scattering models. Like other band-model methods, the *k*-distribution approach is developed for a homogeneous path. However, for nonhomogeneous atmospheres, we must use the one-parameter scaling approximation, which can lead to large deviations from results computed from line-by-line methods (LBL).

Corresponding author address: Professor K. N. Liou, Department of Meteorology, University of Utah, 809 William C. Browning Bldg., Salt Lake City, UT 84112.

Furthermore, the treatment of Doppler broadening becomes difficult in the upper atmosphere because the reference pressure and temperature in the k distribution must be set in the troposphere.

The correlated k-distribution method (CKD) is an extension of the k distribution to nonhomogeneous paths first proposed by Lacis et al. (1979). In this method, the vertical nonhomogeneity of the atmosphere is accurately accounted for by assuming a simple correlation of k distributions at different temperatures and pressures. Since the CKD approach allows us to make use of k distributions at each altitude, the appropriate Voigt profile can also be accounted for throughout the atmosphere. Like the k-distribution method, the CKD approach can be used for absorption bands in both solar and thermal infrared spectra and, at the same time, the results from this method can be directly incorporated into multiple-scattering processes associated with cloud and aerosol particles.

Goody et al. (1989) have presented a formal proof of the validity of CKD under the limits of strong- and weak-line absorption and used the multiplication property of transmittances for application to overlap bands. The accuracy of CKD for flux calculations has been examined in the spectral intervals 5000–5050 cm^{-1} and 1040–1070 cm^{-1} for $H_2O(CO_2)$ and O_3, respectively. Errors due to CKD with respect to LBL results are generally on the order of 1%. Recently, Lacis and Oinas (1991) reported a detailed testing of CKD. Malkmus band parametric fits, based on LBL calculations, were used to derive the k distributions. The overlap bands were treated in terms of the single Malkmus band model by combining the parameters for each gas. By comparing their findings with LBL results, Lacis and Oinas also illustrated that the CKD is capable of achieving numerical accuracy to within 1%.

In spite of a number of advantages in CKD, this method has not yet been widely accepted and used in numerical models in comparison with band models and scaling approximations. From our perspective, the lack of recognition may be due to the following reasons: 1) the physical and mathematical validity of CKD has not been defined precisely and clearly; 2) parameterization to incorporate temperature and pressure effects in the k-distribution function is too complicated; and 3) the treatment of the overlap of absorption bands is either time consuming or inaccurate. In addition, some aspects of the CKD approach have not been discussed thoroughly in the literature. Little attention has been given to the explanation of the errors in CKD, the application of this approach to absorption bands in the solar spectrum, or the use of the optimum number of quadrature points in numerical integration. We wish to further examine CKD with respect to its physical and mathematical foundation and with reference to the preceding problems.

In section 2, we formulate the CKD approach theoretically, and identify the mathematical and physical conditions under which this method is valid. The parameterization for incorporating pressure and temperature effects in the k distribution is subsequently presented in section 3. In section 4, we examine the errors of CKD for absorption bands in both solar and thermal infrared spectra and investigate the errors due to both the CKD method and the use of the optimum number of quadrature points. In section 5, we develop an overlap treatment for various absorption bands that will provide high efficiency and accuracy. Finally, conclusions are given in section 6.

2. A discussion on the correlated k-distribution method

The absorption coefficient is a function of wavenumber, pressure, and temperature, and can be written in the form

$$k(\nu, p, T) = \sum_i S_i(T) f_i(\nu, p, T), \qquad (2.1)$$

where S_i is the line intensity for the ith absorption line and f_i is the normalized line shape. Consider the homogeneous condition under which pressure and temperature are constant. For a given absorption gas and spectral interval, $\Delta\nu$, we may introduce the k-distribution function $h(k)$, which is the probability density function such that $h(k)dk$ is the fraction of $\Delta\nu$ within which the absorption coefficient is between k and $k + dk$. Thus, the spectral-mean transmittance should depend on the k distribution but is independent of the ordering of the absorption coefficients, $k(\nu)$, with respect to the wavenumber (Ambartzumian 1936; Arking and Grossman 1972). We may replace the wavenumber integration by an integration over the k space. Let the maximum and minimum absorption coefficients within $\Delta\nu$ be k_{max} and k_{min}. Setting $k_{min} \to 0$ and $k_{max} \to \infty$ for mathematical convenience, the spectral-mean transmittance as a function of pathlength, u, may be expressed by

$$T_{\bar{\nu}}(u) = \int_{\Delta\nu} e^{-k(\nu)u} \frac{d\nu}{\Delta\nu} = \int_0^\infty e^{-ku} h(k)dk, \qquad (2.2)$$

where $h(k)$ is normalized to 1 in the domain $(0, \infty)$. Equation (2.2) defines the k-distribution approach, which is exact for the homogeneous case. We may further define a cumulative probability function in the form

$$g(k) = \int_0^k h(k)dk, \qquad (2.3)$$

where $g(0) = 0$, $g(k \to \infty) = 1$, and $dg(k) = h(k)dk$. By definition, $g(k)$ is a monotonically increasing and smooth function in k space. It follows that the spectral-mean transmittance can now be expressed in terms of cumulative probability g in the form

$$T_{\bar{\nu}}(u) = \int_{\Delta\nu} e^{-k(\nu)u} \frac{d\nu}{\Delta\nu} = \int_0^1 e^{-k(g)u} dg, \quad (2.4)$$

where $k(g)$ is referred to as the equivalent k function, which is the inverse function of $g(k)$. Since $g(k)$ is a smooth function in k space, $k(g)$ must also be a smooth function in g space.

In order to apply the k-distribution method to a nonhomogeneous atmosphere, we shall consider this atmosphere defined by the two heights, z_1 and z_2. The spectral-mean transmittance can be written in the form

$$T_{\bar{\nu}} = \int_{\Delta\nu} \exp\left[-\int_{z_1}^{z_2} k(\nu, p, T)\rho dz\right] \frac{d\nu}{\Delta\nu}, \quad (2.5)$$

where ρ is the density of the absorber and we have introduced pressure and temperature dependence in the absorption coefficient. We wish to investigate the physical and mathematical conditions under which Eq. (2.5) may be expressed in a form similar to Eq. (2.4), namely,

$$T_{\bar{\nu}} = \int_0^1 \exp\left[-\int_{z_1}^{z_2} k(g, p, T)\rho dz\right] dg. \quad (2.6)$$

The method for calculating spectral-mean transmittance based on Eq. (2.6) is referred to as the correlated k-distribution method (CKD). In essence, the physical implication of CKD is that only one g exists for a given ν at different heights.

The deduction from Eq. (2.5) to Eq. (2.6) based on the definitions of the cumulative probability function, $g(k, p, T)$, and the equivalent k function, $k(g, p, T)$, is not as straightforward as it appears. In the following, we shall attempt to illustrate the assumptions that are required for the derivation of the correlated k equation.

(i) First, we postulate that the absorption coefficients at two wavenumbers, ν_i and ν_j ($i \neq j$), are the same at any arbitrary pressure and temperature, if they are the same at a reference pressure, p_r, and temperature T_r. This postulation implies that

$$k(\nu_i, p, T) = k(\nu_j, p, T), \text{ if } k_r(\nu_i) = k_r(\nu_j), \quad (2.7a)$$

where k_r denotes the absorption coefficient for the reference condition. It follows that for a given ν, there will be a k_r such that

$$k(\nu, p, T) = \chi[k_r(\nu), p, T], \quad (2.7b)$$

where the symbol χ is the function so defined. Equation (2.7b) also satisfies Eq. (2.7a). Thus, these two equations are equivalent. Substituting Eq. (2.7b) in Eq. (2.5) leads to

$$T_{\bar{\nu}} = \int_{\Delta\nu} \exp\left\{-\int_{z_1}^{z_2} \chi[k_r(\nu), p, T]\rho dz\right\} \frac{d\nu}{\Delta\nu}$$
$$= \int_0^\infty \exp\left[-\int_{z_1}^{z_2} \chi(k_r, p, T)\rho dz\right] h_r(k_r) dk_r, \quad (2.8)$$

where $h_r(k_r)$ is the k-distribution function for the reference condition. The concept of the k-distribution method expressed in Eq. (2.2) has been used for a reference condition denoted by subscript r. On the basis of the cumulative probability function defined in Eq. (2.3), we have $dg_r = h_r(k_r)dk_r$, and $g_r(k_r)$ is a monotonic function of k_r. We may further define a function, β, in the g_r domain such that

$$\chi[k_r(g_r), p, T] = \beta(g_r, p, T), \quad (2.9)$$

where $k_r(g_r)$ is the inverse function of $g_r(k_r)$. Thus, using variable transformation, Eq. (2.8) can be rewritten in the form

$$T_{\bar{\nu}} = \int_0^1 \exp\left[-\int_{z_1}^{z_2} \beta(g_r, p, T)\rho dz\right] dg_r. \quad (2.10)$$

(ii) Second, we postulate that the absorption coefficient at ν_i is larger than the coefficient at ν_j at any arbitrary pressure and temperature, if the absorption coefficient at ν_i is larger than the one at ν_j at a reference pressure and temperature. This postulation implies that

$$k(\nu_i, p, T) > k(\nu_j, p, T), \text{ if } k_r(\nu_i) > k_r(\nu_j). \quad (2.11)$$

Since the cumulative probability function defined in Eq. (2.3) is the fraction of the spectral interval within which the absorption coefficient is smaller than k, under the condition expressed in Eq. (2.11) we must have

$$g_r[k_r(\nu)] = g[k(\nu, p, T), p, T] \quad (2.12)$$

for a given wavenumber ν. Equations (2.11) and (2.12) are equivalent, which states that the ordering of the absorption coefficient with respect to its values is independent of pressure and temperature and that only one g exists for a given ν at different levels. Using Eq. (2.12), Eq. (2.10) may be rewritten in the form

$$T_{\bar{\nu}} = \int_0^1 \exp\left[-\int_{z_1}^{z_2} \beta(g, p, T)\rho dz\right] dg. \quad (2.13)$$

From Eqs. (2.7b), (2.9), and (2.12), we obtain the following relationship:

$$k = \beta[g(k)], \quad (2.14)$$

where the dependent variables ν, p, and T have been omitted for simplicity. Equation (2.14) implies that $\beta(g) = k(g)$, provided that k is a monotonic function in g space. It follows that Eq. (2.13) is equivalent to Eq. (2.6).

Physically, the first postulation provides the basis for the use of the k-distribution method at the reference condition, while the second relates the cumulative probability function at the reference level to that at other levels. It is noted that these two postulations are not mutually exclusive mathematically. However, they are required to prove that Eq. (2.6) is exactly equal to Eq. (2.5). We further note that the first postulation requires less restriction than the second and can be

used independently as a better approximation than CKD. Under the correlated conditions, g may replace ν as an independent variable in transmittance calculations. Figures 1a and 1b show, respectively, the spectral distribution of the absorption coefficient and this coefficient as a function of cumulative probability for the O_3 9.6-μm band at $p = 25$ mb and $T = 220$ K. The wavenumber dependence of the absorption coefficient was obtained by means of line-by-line computations assuming Voigt line shape. It is clear that the absorption coefficient is a rapidly varying function of wavenumber but is a smooth function in the domain of cumulative probability space. Thus, the integration in g space, which replaces the tedious wavenumber integration, can be evaluated by using only a few numerical quadrature points.

Evaluation of spectral-mean transmittance in nonhomogeneous atmospheres requires coupled height and wavenumber integrations [Eq. (2.5)]. Traditionally, these integrations have been separated by some approximations such that band models can be applied. In this spirit, one-parameter scaling, two-parameter Curtis–Godson approximation, and three-parameter scaling (Goody 1964; Yamamoto et al. 1972) are all based on the same philosophy. However, in the CKD approach, after the transformation of ν space to g space, the separation of height and g integrations is not necessary because the height integration can be effectively carried out in g space under the correlated assumptions. The approach fundamentally differs from historical band models and scaling approximations and appears to offer a direct solution to the intricate transfer problem involving nongray gaseous absorption. In the following, we shall investigate both the conditions under which the CKD is valid and its limitations.

a. Single line

Consider a Lorentz line whose absorption coefficient is given by

$$k(\nu, p, T) = \frac{S(T)}{\pi} \frac{\alpha(p, T)}{\nu^2 + \alpha^2(p, T)}, \quad (2.15)$$

where α is the half-width. For any two wavenumbers ν_i and ν_j, if $k_r(\nu_i) = k_r(\nu_j)$, we must have $\nu_i^2 = \nu_j^2$. It follows that $k(\nu_i, p, T) = k(\nu_j, p, T)$, the condition postulated in Eq. (2.7a). If $k_r(\nu_i) > k_r(\nu_j)$, we must have $\nu_i^2 < \nu_j^2$. It follows that $k(\nu_i, p, T) > k(\nu_j, p, T)$, the condition postulated in Eq. (2.11). The same argument can be applied to the Doppler line profile. Therefore, for a single line of any shape, Eq. (2.6) is equivalent to Eq. (2.5). The same result was pointed out by Lacis et al. (1979). Consider a small spectral band within which the absorption lines are randomly distributed such that a generalized single line in terms of the equivalent width may be realized (Goody and Yung 1989). Under this condition, the CKD may also be viewed as exact.

b. Elsasser band model

If a single spectral line repeats itself periodically or regularly, referred to as the Elsasser band model (Elsasser 1938), the absorption coefficient can be written in the form

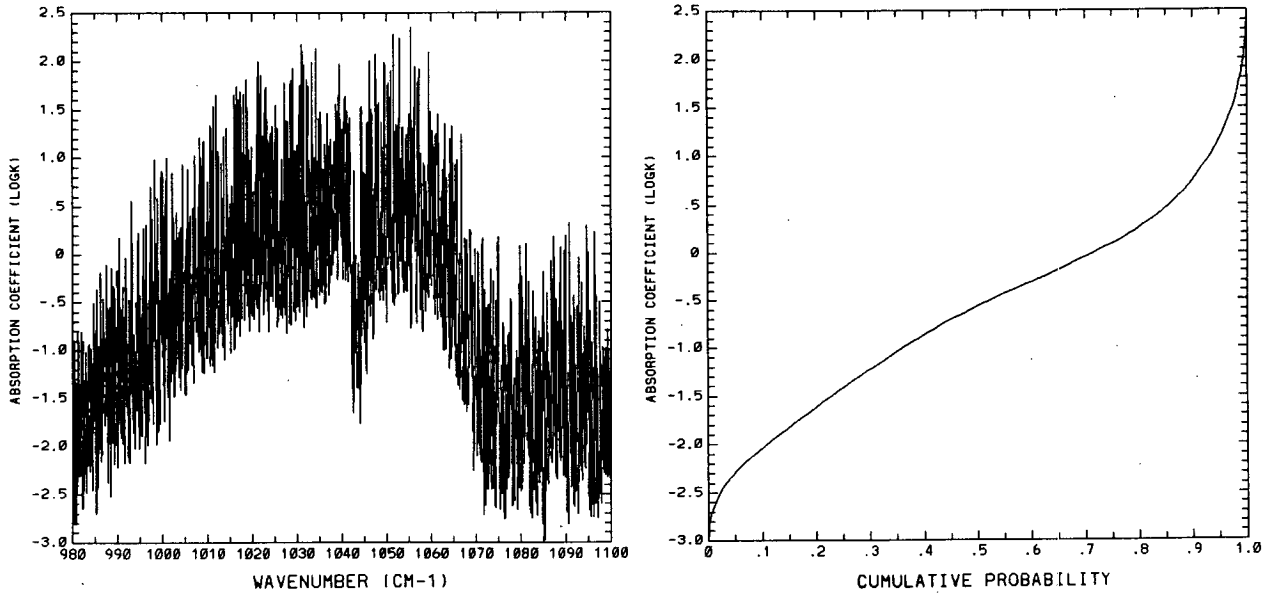

FIG. 1. Absorption coefficient k in (cm atm)$^{-1}$ as a function of (a) wavenumber and (b) cumulative probability for the O_3 9.6-μm band for a pressure of 25 mb and a temperature of 220 K.

$$k(\nu, p, T) = \sum_{n=-\infty}^{\infty} \frac{S(T)}{\pi} \frac{\alpha(p, T)}{(\nu - n\delta)^2 + \alpha^2(p, T)}, \tag{2.16}$$

where δ is the line spacing. From the Mittag–Leffler theorem (Whittacker and Watson 1940), the infinite sum can be expressed in terms of periodic and hyperbolic functions as follows:

$$k(\nu, p, T) = \frac{S(T)}{\delta} \frac{\sinh\beta(p, T)}{\cosh\beta(p, T) - \cos\gamma}, \tag{2.17}$$

where $\beta(p, T) = 2\pi\alpha(p, T)/\delta$, and $\gamma = 2\pi\nu/\delta$. For any two wavenumbers ν_i and ν_j, if $k_r(\nu_i) = k_r(\nu_j)$, we have $\cos\gamma_i = \cos\gamma_j$. This implies that $k(\nu_i, p, T) = k(\nu_j, p, T)$, the condition postulated in Eq. (2.7a). If $k_r(\nu_i) > k_r(\nu_j)$, then $\cos\gamma_i > \cos\gamma_j$. This implies that $k(\nu_i, p, T) > k(\nu_j, p, T)$, the condition postulated in Eq. (2.11). Therefore, CKD is exact for the periodic line model.

c. *Strong-line limits*

Under the strong-line limits, the absorption near the centers of pressure broadened lines becomes saturated. As a good approximation, we may scale the absorption coefficient in the form (Chou and Arking 1980)

$$k(\nu, p, T) \approx k_r(\nu) f(p, T). \tag{2.18}$$

Equation (2.18) satisfies the conditions postulated in Eqs. (2.7a) and (2.11). Thus, under strong-line limits, Eq. (2.6) is equivalent to Eq. (2.5).

d. *Weak-line limit*

Using Eq. (2.1) and under the limits of weak-line absorption, Eq. (2.5) may be expressed by

$$\begin{aligned} T_{\bar{\nu}} &\approx \int_{\Delta\nu} \left[1 - \int_{z_1}^{z_2} \sum_i S_i(T) f_i(\nu, p, T) \rho dz\right] \frac{d\nu}{\Delta\nu} \\ &= 1 - \int_{z_1}^{z_2} \sum_i S_i(T) \rho dz / \Delta\nu \\ &\approx \exp\left[-\int_{z_1}^{z_2} k_{\bar{\nu}}(T) \rho dz\right], \end{aligned} \tag{2.19}$$

where we have defined a gray absorption coefficient, which is a function of temperature only as follows: $k_{\bar{\nu}}(T) = \sum_i S_i(T)/\Delta\nu$. Thus, under the weak-line limits, we may replace $k(\nu, p, T)$ by $k_{\bar{\nu}}(T)$. Consequently, $k(\nu_i, p, T) = k(\nu_j, p, T) = k_{\bar{\nu}}(T)$, if $k_r(\nu_i) = k_r(\nu_j) = k_{\bar{\nu}}(T_r)$. Thus, the condition postulated in Eq. (2.7a) is satisfied. Since $k_{\bar{\nu}}(T)$ is constant over $\Delta\nu$, the condition postulated in Eq. (2.11) does not apply. We may argue that this condition is also satisfied by weak-line limits.

e. *General absorption spectrum*

The preceding discussion demonstrates that the correlated k-distribution method is correct for four specific cases. The CKD for transmittance calculations over nonhomogeneous atmosphere is clearly superior to the Curtis–Godson two-parameter approximation. This is because the CKD can exactly apply to a single absorption line, while the Curtis–Godson approximation is valid only for strong- and weak-line limits. In the following, we wish to investigate the deviations of the correlated assumptions for the realistic absorption spectrum. These deviations occur because of partial line overlap, the difference of half-widths and strengths for absorption lines, and the nonunique temperature dependence of line strength. The deviations (referred to here as blurring) of the correlated conditions due to pressure and temperature differences are illustrated using a large number of wavenumbers in the H_2O 400–540 cm^{-1} spectral region. The cumulative probability functions at two different levels are denoted as g_1 and g_2 (see the next section for the evaluation of g). In Fig. 2, the point is defined by $(g_1, g_2) = \{g[k(\nu, p_1, T), p_1, T], g[k(\nu, p_2, T), p_2, T]\}$, where the temperature is fixed at 273 K, but pressure varies from $p_1 = 1000$ mb to $p_2 = 631$ mb in (a), and from $p_1 = 1000$ mb to $p_2 = 251$ mb in (b). In Fig. 3, the point is defined by $(g_1, g_2) = \{g[k(\nu, p, T_1), p, T_1], g[k(\nu, p, T_2), p, T_2]\}$, where the pressure is fixed at 1000 mb, but temperature varies from $T_1 = 300$ K to $T_2 = 273$ K in (a), and from $T_1 = 300$ K to $T_2 = 245$ K in (b). Under the postulations defined in Eqs. (2.7a) and (2.11), $g_1 = g_2$ for a given ν and all points should lie on the diagonal line. We define ϵ as the absolute root-mean-square (rms) difference for g_1 and g_2, which is a measure of the degree of blurring produced by the two postulations. The values of ϵ are displayed in Figs. 2 and 3. In general, blurring is enhanced when the two levels are far apart, implying that the correlated conditions are better assumptions for two closer levels. Comparing Figs. 2 and 3, we find that the temperature effects produce more blurring than the blurring produced by pressure in the troposphere. It is noted that the two levels depicted in Figs. 2 and 3 are separated by large distances [~4 and 9 km in (a) and (b), respectively]. We anticipate that the correlated conditions should be an excellent approximation for flux and heating rate calculations since the most significant flux exchanges take place in adjacent levels (Wu 1980; Chou and Kouvaris 1991). The effects of the blurring on the flux and heating rate calculations will be discussed in section 4. Deviations of the correlated conditions have also been studied by West et al. (1990) and Lacis and Oinas (1991) by mapping the spectrum onto g and ν space, respectively. West et al. have developed an improved spectral mapping approach that does not require the correlated conditions in the transmittance calculation.

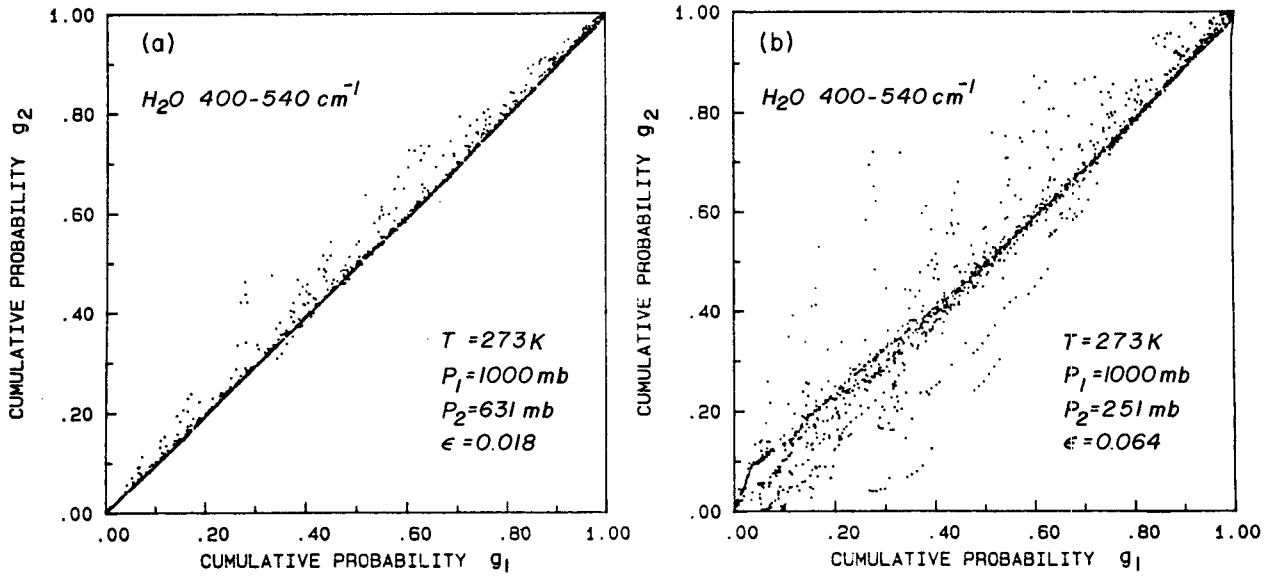

FIG. 2. Blurring of the correlated assumptions due to the pressure effect for H_2O in the spectral region 400–540 cm^{-1} at a temperature T = 273 K. The point is defined by $(g_1, g_2) = \{g[k(\nu, p_1, T), p_1, T], g[k(\nu, p_2, T), p_2, T]\}$ at different wavenumbers. In (a) p_1 = 1000 mb and p_2 = 631 mb, and in (b) p_1 = 1000 mb and p_2 = 251 mb. The value ϵ is the absolute rms difference.

3. Computation of absorption coefficients and equivalent k functions

The absorption coefficient for a given wavenumber and particular gas has been defined in Eq. (2.1). The temperature dependence of the line intensity may be obtained from quantum theory. As a good approximation, we have

$$S_i(T) \approx S_i(T_0)\left(\frac{T_0}{T}\right)^m \times \frac{Q_v(T_0)}{Q_v(T)} \frac{1-\exp(-hc\nu_{ij}/KT)}{1-\exp(-hc\nu_{ij}/KT_0)} \times \exp\left[-\frac{hcE_i}{K}\left(\frac{1}{T}-\frac{1}{T_0}\right)\right], \quad (3.1)$$

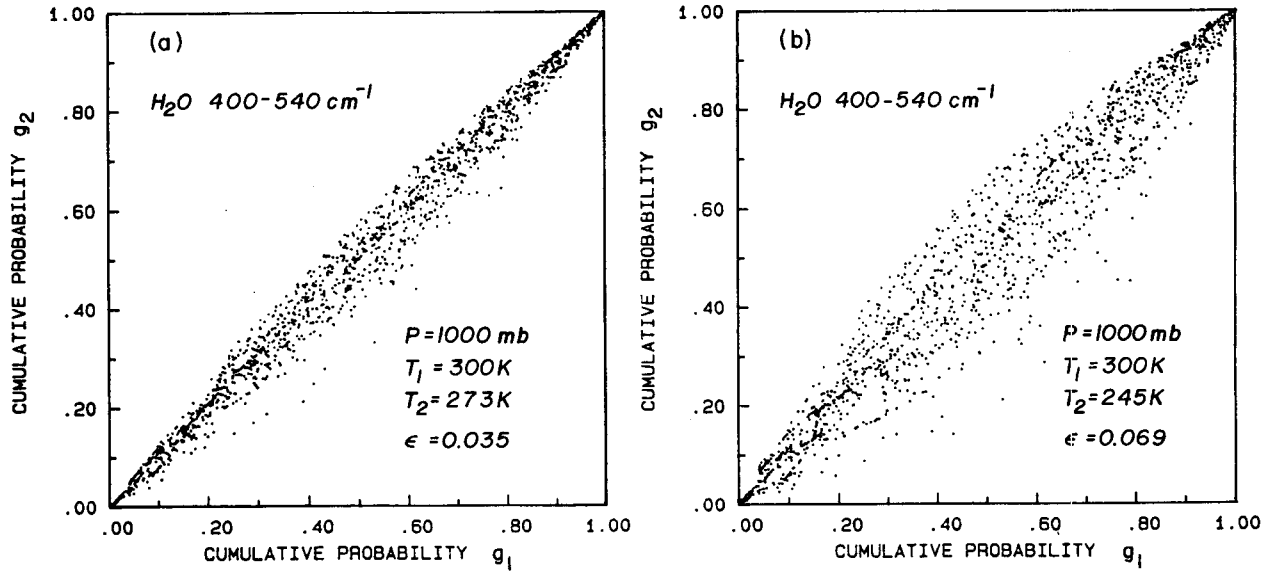

FIG. 3. Blurring of correlated assumptions due to the temperature effect for H_2O in the spectral region 400–540 cm^{-1} at a pressure p = 1000 mb. The point is defined by $(g_1, g_2) = \{g[k(\nu, p, T_1), p, T_1], g[k(\nu, p, T_2), p, T_2]\}$ at the different wavenumbers. In (a) T_1 = 300 K and T_2 = 273 K and in (b) T_1 = 300 K and T_2 = 245 K. The value ϵ is the absolute rms difference.

where $T_0 = 296$ K, $m = 1.5$ and 1.0 for nonlinear and linear molecules, respectively, Q_v is the vibrational partition function that is close to 1 (McClatchey et al. 1973), ν_{ij} is the wavenumber for the line center, E_i is the energy of lower state, h is the Planck constant, K is the Boltzmann constant, and c is the velocity of light. For the Lorentz line shape, the half-width is given by

$$\alpha_i(p, T) = \alpha_i(p_0, T_0)\left(\frac{p}{p_0}\right)\left(\frac{T_0}{T}\right)^n, \quad (3.2)$$

where p_0 and T_0 are set at 1 atm and 296 K. The temperature-dependent index $n = 0.64, 0.75, 0.76$, and 1.0 for H_2O, $CO_2(N_2O)$, O_3, and CH_4, respectively (Rothman et al. 1986).

To compute the absorption coefficient, the line parameters were taken from the 1982 version of the AFGL data type (Rothman et al. 1983). Also, the Voigt line shape was used in the computation. Following the work of Chou and Kouvaris (1986), the spectral resolutions used were 0.002 cm^{-1} in the 540–800 cm^{-1} CO_2 spectral region, 0.005 cm^{-1} in the 980–1100 cm^{-1} O_3 spectral region and the bands involving CH_4 and N_2O, and 0.01 cm^{-1} in the entire thermal infrared H_2O spectral region. For the solar spectrum, a resolution of 0.025 cm^{-1} was used for H_2O bands. The lines were cut off at 260 times the Lorentz half-width from line centers. In the region of very low pressure, the cutoff wavenumber, ν_c, may be comparable to or smaller than the Doppler half-width, α_D. To ensure that $\nu_c \geq \alpha_D$, we set $\nu_c = \nu_c(p_c)$ for $p < p_c$ where p_c is taken to be 10 and 100 mb for lines at thermal infrared and solar near-infrared regions, respectively. In the computations, we use three temperatures of 200, 250, and 300 K, along with 19 (11) pressures with $\Delta \log_{10} p = 0.2$ for the thermal infrared (solar) calculations.

To facilitate the computation of absorption coefficients for any pressures and temperatures, the following parameterization equation is used (Chou and Kouvaris 1986):

$$\ln k(\nu, p, T) = \sum_{n=0}^{2} a_n(\nu, p)(T - 250)^n. \quad (3.3)$$

For a given wavenumber and pressure, the three preceding temperature values can be used to determine the coefficients $a_n(\nu, p)$ $(n = 0, 1, 2)$, which have been tabulated at 19 (or 11) pressures for the wavenumber resolutions described previously. The absorption coefficients at other pressures can be interpolated linearly in the pressure coordinate.

Next, we discuss the direct computation of the cumulative probability function, $g(k, p, T)$, from $k(\nu, p, T)$. For a given absorption gas and spectral region, $\Delta\nu$, if the absorption coefficients are computed using a spectral resolution δ (e.g., 0.002 cm^{-1} in the 15-μm CO_2 band), the total number of computational points will be $N = \Delta\nu/\delta$. We define the number of wavenumber points at which the absorption coefficients, $k(\nu, p, T)$, are between 0 and k as $n(0, k; p, T)$. Thus, the cumulative probability function is given by

$$g(k, p, T) = n(0, k; p, T)/N. \quad (3.4)$$

This provides a direct relation between k and g. For numerical computations in g space, we use the intervals 0.01 and 0.001 for g from 0 to 0.95 and from 0.95 to 1, respectively; the higher resolution in the latter case is chosen to resolve the sharply peaked equivalent k function in the upper atmosphere. The total number of g values is 145, which is "exact" in numerical integration. Figures 4a and 4b show $k(g, p, T)$ as a function of g for the CO_2 540–670 cm^{-1} spectral interval for a fixed temperature and pressure, respectively.

In the preceding procedures, $k(g, p, T)$ is calculated exactly at three temperatures and 19 (or 11) pressures. In order to utilize CKD for transmittance calculations, we must develop a methodology to compute $k(g, p, T)$ at arbitrary pressures and temperatures. Given the conditions under which the correlated k distribution is valid, the cumulative probability function g is equivalent to wavenumber ν. Consequently, interpolations of the absorption coefficient at a given ν with respect to pressure and temperature can be applied to the equivalent k function at a given g, namely,

$$\ln k(g, p, T) = \sum_{n=0}^{2} A_n(g, p)(T - 250)^n. \quad (3.5)$$

Again, the coefficients, $A_n(g, p)$ $(n = 0, 1, 2)$, can be determined by the three temperature values for a given g and p and have been tabulated at 19 (or 11) pressures for 145 g values. The equivalent k function at other pressures can be obtained by linear interpolation in the pressure coordinates. Equation (3.5) is equivalent to Eq. (3.3) under the correlated conditions. It follows that the accuracy of the fitting should also be equivalent. The efficiency of flux and heating rate calculations is obviously dependent on the integration points and will be discussed in the next section.

4. Comparison of the correlated *k*-distribution and line-by-line methods for flux and heating rate calculations

a. Thermal infrared radiation

Consider a relatively narrow spectral interval, $\Delta\nu_i$. The upward and downward fluxes in the height coordinate may be expressed by (Liou 1980)

$$F_\nu^\uparrow(z) = \int_{\Delta\nu_i} F_\nu^\uparrow(z)d\nu,$$

$$= \pi B_\nu(T_s)T_\nu^f(0, z) + \int_0^z \pi B_\nu[T(z')]\frac{d}{dz'}T_\nu^f(z', z)dz', \quad (4.1a)$$

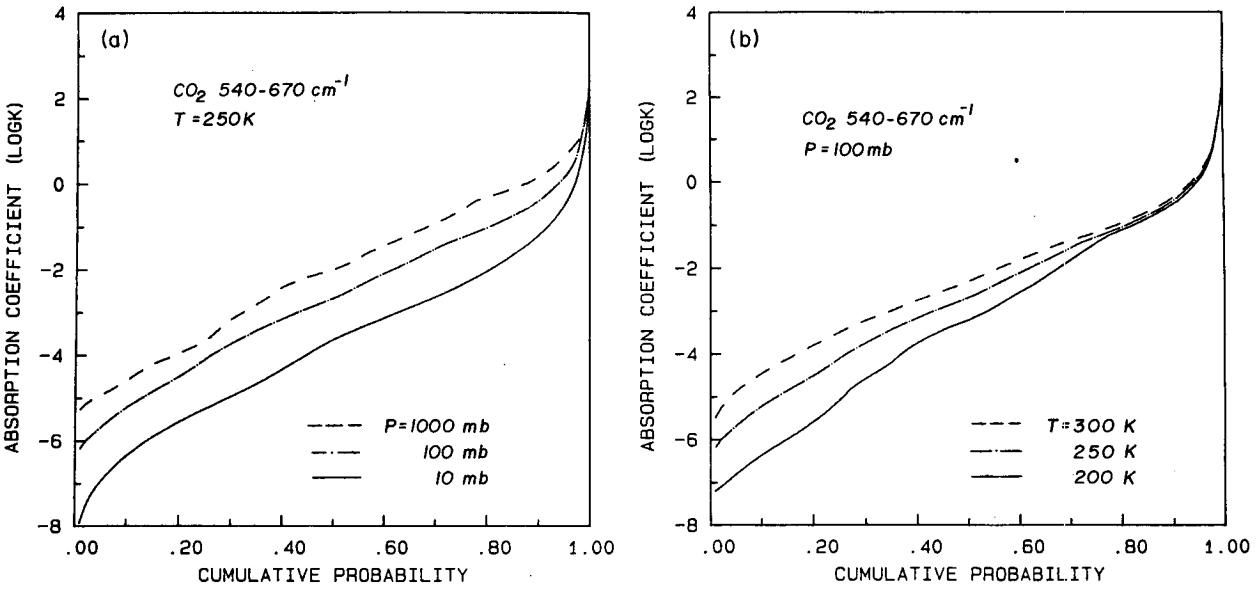

FIG. 4. The absorption coefficient in (cm atm)$^{-1}$ as a function of the cumulative probability g for the CO_2 540–670 cm^{-1} spectral region (a) for a temperature of 250 K with three pressures and (b) for a pressure of 100 mb with three temperatures.

$$F_{\bar{\nu}}^{\downarrow}(z) = \int_{\Delta\nu_i} F_{\nu}^{\downarrow}(z)d\nu = \int_{z_\infty}^{z} \pi B_{\bar{\nu}}[T(z')] \frac{d}{dz'} T_{\bar{\nu}}^{f}(z, z')dz', \quad (4.1b)$$

where $B_{\bar{\nu}}$ is the spectrally integrated Planck function, z_∞ is the height at TOA, T_s is the surface temperature, and the diffuse spectral-mean transmittance between levels z and z' is defined by $T_{\bar{\nu}}^{f}(z, z') = 2\int_0^1 T_{\bar{\nu}}(z, z'; \mu)\mu d\mu$. The spectral-mean transmittances based on the LBL and CKD methods are, respectively, given by

$$T_{\bar{\nu}}(z, z'; \mu) = \int_{\Delta\nu_i} \exp\left[-\int_z^{z'} k(\nu, p, T)\rho \frac{dz''}{\mu}\right] \frac{d\nu}{\Delta\nu_i}, \quad (4.2)$$

$$T_{\bar{\nu}}(z, z'; \mu) = \int_0^1 \exp\left[-\int_z^{z'} k(g, p, T)\rho \frac{dz''}{\mu}\right] dg. \quad (4.3)$$

The net flux $F_{\bar{\nu}} = F_{\bar{\nu}}^{\uparrow} - F_{\bar{\nu}}^{\downarrow}$. The heating rate is then calculated from the divergence of the net flux.

In the calculations, we divide the entire infrared absorption spectrum between 0 and 2200 cm^{-1} into 12 subspectral intervals according to the positions of various absorption bands: 0–280, 280–400, 400–540, 540–670, 670–800, 800–980, 980–1100, 1100–1250, 1250–1400, 1400–1700, 1700–1900, and 1900–2200 cm^{-1}. Variations of the Planck function in these intervals are sufficiently small and may be assumed to be constant. The angular integration was carried out with a fourth-order Gaussian quadrature. In the vertical, the atmosphere was equally divided into 60 homogeneous layers between the surface and TOA, set at 60 km. Four atmospheric profiles, including midlatitude summer, subarctic winter, tropical and U.S. Standard atmospheres (McClatchey et al. 1971) were used in the flux and heating rate calculations. The temperature, the ozone mixing ratio, and the logarithm of pressure and water vapor mixing ratio are assumed to be linear in the height coordinate. The CO_2, CH_4, and N_2O mixing ratios are assumed to be uniform throughout the atmosphere with concentrations of 330, 1.6, and 0.28 ppmv, respectively. It is noted that the truncation of the atmosphere at 60 km can produce artificially large cooling rates near TOA. However, this truncation does not affect the comparison of LBL and CKD.

Table 1 shows comparisons of the downward flux at the surface and the upward flux at TOA between CKD and LBL for four atmospheric conditions and three principal absorbing gases (H_2O, CO_2, and O_3). Contributions from the water vapor continuum are excluded from the calculations. The downward surface and TOA fluxes associated with H_2O computed from CKD do not differ from those computed from LBL by more than 0.2 and 0.05%, respectively. Fluxes produced by CO_2 using CKD agree with those computed from LBL within 0.2% for every case. For the O_3 9.6-μm bands, fluxes computed from CKD produce relatively larger errors than those associated with CO_2 and H_2O bands; ~2.5% in $F^{\downarrow}(0)$ and ~1.5% in $F^{\uparrow}$(TOA). This is because the O_3 9.6-μm band exhibits a large number of intermediate absorption lines. However, the CKD achieves a much higher accuracy than the Curtis–Godson (C–G) scaling, which may lead to flux errors of up to 10% for the O_3 9.6-μm band (Kratz and Cess 1988; Fu 1991). Comparisons of the results computed from

TABLE 1. Comparison of the line-by-line and correlated k-distribution methods for radiative fluxes (W m^{-2}) at the top and surface due to individual gases in the infrared spectrum. The percentage error is in parentheses.

	$F^{\downarrow}$ (0)			$F^{\uparrow}$ (TOA)		
	LBL	CKD	CKDA	LBL	CKD	CKDA
			H_2O (lines only) 0–2200 cm^{-1}			
MLS*	262.65	262.20 (−0.17)	263.68 (0.39)	334.85	334.97 (0.04)	334.43 (−0.12)
SAW*	119.29	119.16 (−0.11)	120.07 (0.65)	224.55	224.57 (0.01)	224.46 (−0.04)
TRO*	293.83	293.29 (−0.19)	296.27 (0.83)	351.40	351.56 (0.05)	350.86 (−0.15)
USS*	215.80	215.44 (−0.17)	216.58 (0.36)	311.55	311.64 (0.03)	311.12 (−0.14)
			CO_2 540–800 cm^{-1}			
MLS	73.54	73.45 (−0.12)	73.81 (0.37)	74.51	74.65 (0.19)	74.53 (0.03)
SAW	43.73	43.66 (−0.16)	43.45 (−0.64)	52.26	52.33 (0.13)	52.29 (0.06)
TRO	78.73	78.65 (−0.10)	79.17 (0.56)	75.88	76.04 (0.21)	75.87 (−0.01)
USS	66.37	66.30 (−0.11)	66.30 (−0.11)	69.10	69.23 (0.19)	69.18 (0.12)
			O_3 980–1100 cm^{-1}			
MLS	4.54	4.42 (−2.6)	4.48 (−1.3)	22.80	23.15 (1.5)	22.95 (0.66)
SAW	2.86	2.80 (−2.1)	2.86 (0.0)	10.92	11.02 (0.92)	10.91 (−0.09)
TRO	3.67	3.58 (−2.4)	3.62 (−1.4)	26.89	27.22 (1.2)	27.15 (0.97)
USS	3.44	3.35 (−2.6)	3.40 (−1.2)	20.50	20.79 (1.4)	20.62 (0.58)

* MLS, SAW, TRO, and USS are abbreviations for midlatitude summer, subarctic winter, tropical, and U.S. Standard atmospheres, respectively.

CKD and LBL show that the errors in $F^{\downarrow}(0)$ are always negative, whereas the errors in $F^{\uparrow}(\text{TOA})$ are always positive. The reason for the systematic errors may be explained by the following. The absorption coefficient over a spectral interval $\Delta\nu$ has a finite number of maxima and minima. Under the correlated conditions, the positions of maxima and minima are maintained regardless of pressure and temperature variations. For this reason, the CKD overestimates and underestimates the absorption in the vicinity of maxima and minima, respectively. Since absorption is generally saturated at the maxima, underestimation of absorption near the minima predominates. As a result, the correlated equation [Eq. (2.6)] may overestimate the spectral-mean transmittance, leading to more transparent atmosphere. This suggests that for thermal radiation, CKD would underestimate the downward surface flux but overestimate the flux at TOA. Comparisons in Table 1 demonstrate that the blurring of the correlated assumptions has little impact on the flux calculation.

Figures 5a, 5c, and 5e show the heating rate profiles computed from LBL for H_2O (0–2200 cm^{-1}), CO_2 (540–800 cm^{-1}), and O_3 (980–1100 cm^{-1}), respectively. Figures 5b, 5d, and 5f show the corresponding error profiles for the results computed from CKD. From LBL results, we see that infrared cooling rates in the troposphere are primarily produced by H_2O. In the stratosphere, H_2O, CO_2, and O_3 contribute ~15%, 70%, and 15% of the total cooling in the vicinity of the 50-km region, respectively. For H_2O, errors in the heating rates calculated by CKD are less than ~0.01 K day^{-1} in the troposphere and stratosphere, and less than ~0.24 K day^{-1} above the stratopause, as shown in Fig. 5b. The relatively large errors above stratopause may be explained as follows: At lower pressure regions the atmosphere is thinner and more transparent; as a result, distant layers would affect the cooling more significantly. As shown in Fig. 5d, errors of the CO_2 cooling rates produced by CKD in the troposphere and lower stratosphere are ~0.01 K day^{-1}, while the errors above 30 km are less than ~0.1 K day^{-1}. For O_3, the heating rates computed from CKD are also in excellent agreement with those from LBL. The differences are less than ~0.1 K day^{-1} (Fig. 5f). We further note that CKD obtains best results in the subarctic winter atmosphere both for fluxes and cooling rates due to the O_3 9.6-μm band, as shown in Table 1 and Fig. 5f. This can be explained by the larger amount of ozone in the subarctic winter atmosphere, which leads to stronger absorption and more opaque atmosphere.

The heating of the total atmosphere is a function of the term, $H = F^{\uparrow}(0) - F^{\downarrow}(0) - F^{\uparrow}(\text{TOA})$. From Table 1, we have $\Delta H = H(\text{CKD}) - H(\text{LBL}) \sim 0.3$ W m^{-2} for H_2O. This explains why positive errors predominate in Fig. 5b. For O_3, $\Delta H \sim -0.2$ W m^{-2}. Thus, errors in the heating rate are largely negative (Fig. 5f). For CO_2, $\Delta H \sim 0$. Errors in the heating rate due to CO_2 are slightly negative below 18 km and slightly positive above this height (Fig. 5d). The signs of ΔH appear to be associated with the vertical distribution of absorbing gases.

We have also made comparisons for CH_4 and N_2O absorption in the spectral region 1100–1400 cm^{-1}. Errors resulting from CKD for flux calculations are only on the order of 0.05%, much better than those obtained in the case of O_3. This is because absorption due to CH_4 or N_2O is relatively weak so that CKD gives correct results. For CH_4 and N_2O, errors in cooling rates are both less than 0.01 K day^{-1}.

In CKD, we have used 145 g values in numerical integration. We wish to examine the optimum number of g values that would limit the flux and heating rate results within ~ ±1% below ~40 km for H_2O, CO_2, and O_3 bands. This method is referred to as CKDA. Thus, errors in CKDA are due not only to the blurring of the correlated assumptions, but also to the use of quadrature points. Table 2 lists the optimum number of quadrature points in g.

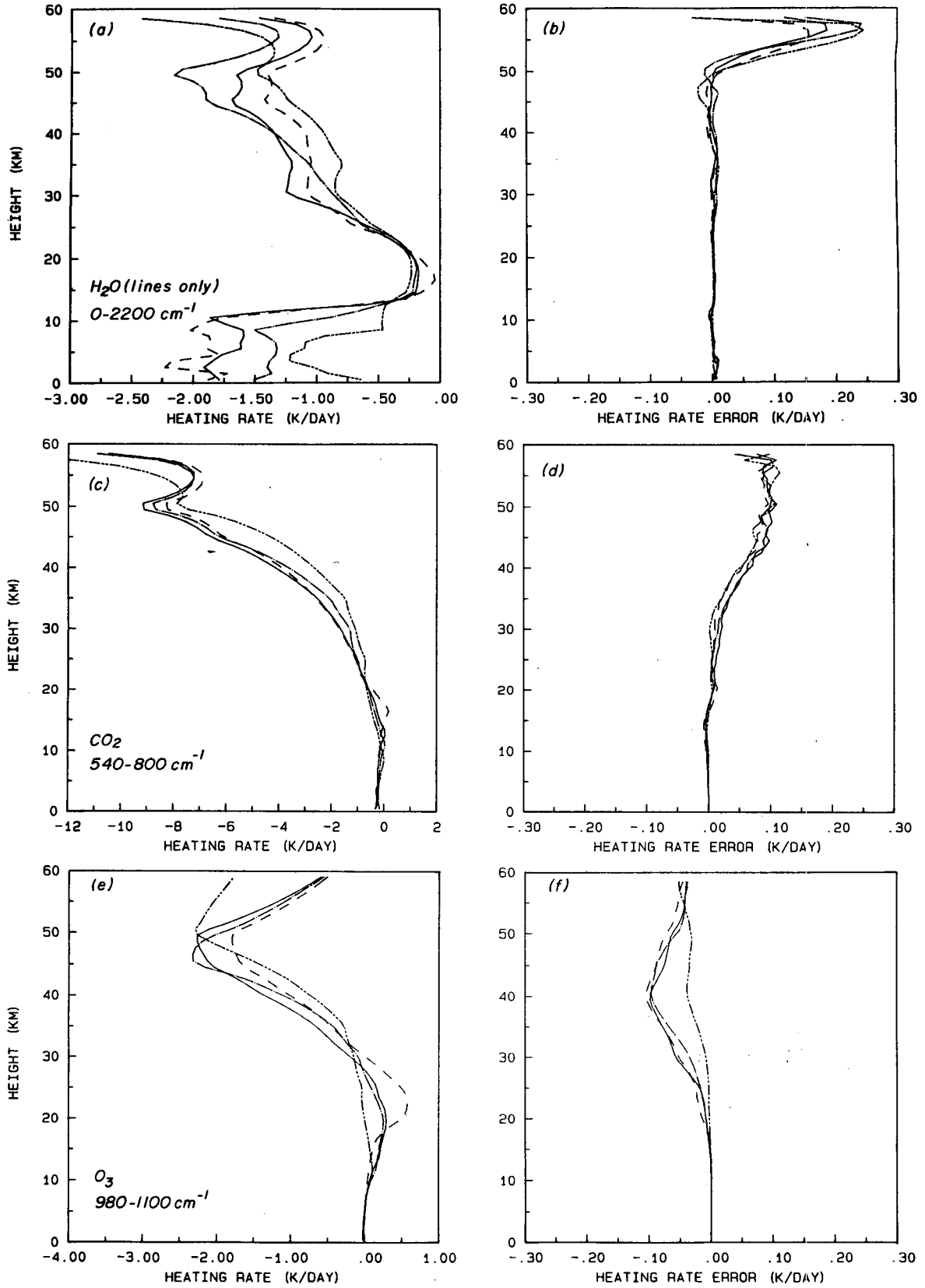

FIG. 5. Heating rate profiles computed from LBL and the error profiles produced by CKD for the (a and b) H_2O, (c and d) CO_2, and (e and f) O_3 bands in the infrared spectrum for the midlatitude summer (solid), subarctic winter (double dot-dashed), tropical (dashed), and *U.S. Standard* (dot-dashed) atmospheres.

TABLE 2. The optimum number of g values in the correlated k-distribution method (see text for the definition of "optimum").

Spectral region (cm^{-1})	Number of quadrature points: H_2O (Lines only)	CO_2	O_3	CH_4	N_2O	H_2O (Continuum)
	Infrared spectrum					
0–280	8					
280–400	7					1
400–540	7					1
540–670	5	10				1
670–800	4	8				1
800–980	2					1
980–1100	1		5			1
1100–1250	3			1	1	1
1250–1400	4			1	1	
1400–1700	4					
1700–1900	3					
1900–2200	2					
	Solar spectrum					
2500–2850	5					
2850–4000	12					
4000–5250	7					
5250–7700	12					
7700–14 500	8					

Comparisons of the LBL and CKDA results for fluxes are also listed in Table 1. For H_2O lines in the spectral region 0–2200 cm^{-1}, the surface and TOA fluxes computed from CKDA agree with those from LBL within ~0.8% and 0.15%, respectively. Using CKDA for the CO_2 15-μm band, the relative errors are within 0.7% and 0.1% for the surface and TOA fluxes, respectively. For the O_3 9.6-μm band, flux accuracies are within ~1% using only 5 g values. CKDA obtains better results than CKD in this case, because errors due to the correlated assumptions are partly offset by those produced by the reduced number of g points in numerical integration. From Table 1 we see that $F^{\downarrow}(0)$ is more sensitive to the number of g points than $F^{\uparrow}(\text{TOA})$.

Figure 6 shows the heating rate error profiles produced by CKDA for the principal absorbing gases in four different atmospheres. Below ~40 km, CKDA can achieve accuracies within about 0.15, 0.05, and 0.1 K day^{-1} for H_2O, CO_2, and O_3 bands, respectively.

For CH_4 and N_2O in the spectral region 1100–1400 cm^{-1}, we use one g for each spectral band (1100–1250 cm^{-1} and 1250–1400 cm^{-1}), as shown in Table 2. This will produce an error in downward surface flux as large as about 10%, which is about 0.75 W m^{-2} in the tropical atmosphere for CH_4 and 0.6 W m^{-2} for N_2O. However, errors in the CH_4 7.7-μm and N_2O 7.8-μm bands will be greatly suppressed by the strong overlap absorption due to H_2O. Note that the use of only one g for both CH_4 and N_2O would make it much more convenient to treat the overlap effects (H_2O + CH_4 + N_2O) in scattering atmospheres.

b. Solar radiation

We shall consider a nonscattering atmosphere in which absorption is primarily due to water vapor. We shall further consider a small spectral interval, $\Delta\nu_j$, such that the spectral solar flux may be taken as constant. Under these conditions and letting the incident solar flux be $S_j\Delta\nu_j$, the downward solar flux at a given level z can be written in the form

$$F_j^{\downarrow}(z) = \mu_0 S_j T_j(z/\mu_0)\Delta\nu_j, \tag{4.4}$$

where μ_0 is the cosine of the solar zenith angle and the spectral-mean transmittance is defined by

$$T_j(z/\mu_0) = \int_{\Delta\nu_j} \exp\left[-\int_z^{\infty} k(\nu, p, T)\rho \frac{dz'}{\mu_0}\right]\frac{d\nu}{\Delta\nu_j}. \tag{4.5a}$$

Transmittance computations can be performed line by line.

Under the correlated conditions, transmittance may be computed in g space in the form

$$T_j(z/\mu_0) = \int_0^1 \exp\left[-\int_z^{\infty} k_j(g, p, T)\rho \frac{dz'}{\mu_0}\right]dg. \tag{4.5b}$$

To facilitate the computation using CKD, we divide the solar spectrum into five bands associated with water vapor absorption: 2500–2850, 2850–4000, 4000–5250, 5250–7700, and 7700–14 500 cm^{-1}. The scattering and absorption properties of cloud and aerosol particles may be treated as constant in these regions. Let the spectral interval for these bands be denoted as $\Delta\nu$, which contains a number of $\Delta\nu_j$. The wavenumber dependence of the spectral solar flux may be taken into account by defining the cumulative probability function for each band in the form

$$g(k, p, T) = \sum_j S_j g_j(k, p, T)\Delta\nu_j/S_{\bar{\nu}}, \tag{4.6}$$

where $S_{\bar{\nu}} = \sum_j S_j\Delta\nu_j$. Subsequently, the flux-weighted equivalent k function can be obtained by inverting $g(k, p, T)$. In this manner, the downward solar flux corresponding to each water vapor band may be written as follows:

$$F_{\bar{\nu}}^{\downarrow}(z) = \mu_0 S_{\bar{\nu}} T_{\bar{\nu}}(z/\mu_0), \tag{4.7}$$

where

$$T_{\bar{\nu}}(z/\mu_0) = \int_0^1 \exp\left[-\int_z^{\infty} k(g, p, T)\rho dz'/\mu_0\right]dg. \tag{4.8}$$

In the calculations of $g(k, p, T)$ for each band, $\Delta\nu_j$

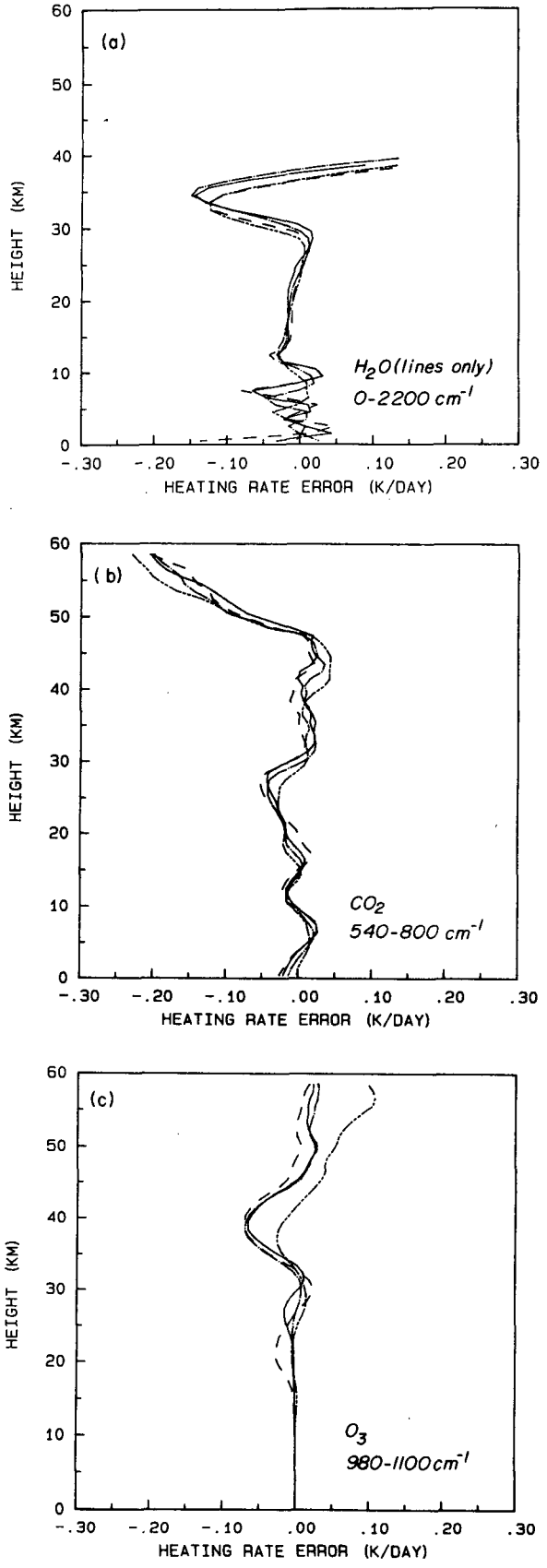

FIG. 6. The error profiles produced by CKDA for the (a) H_2O, (b) CO_2, and (c) O_3 bands in the infrared spectrum for the midlatitude summer (solid), subarctic winter (double dot-dashed), tropical (dashed), and *U.S. Standard* (dot-dashed) atmospheres.

TABLE 3. Comparison of the line-by-line and correlated k-distribution methods for the surface and absorbed fluxes (W m^{-2}) due to H_2O in the solar spectral region 2500–14 500 cm^{-1} with a solar zenith angle of 60°. The percentage error is in parentheses.

	$F^{\downarrow}(0)$			F_a		
	LBL	CKD	CKDA	LBL	CKD	CKDA
MLS	253.29	253.43 (0.06)	253.30 (0.00)	106.87	106.73 (−0.13)	106.86 (−0.01)
SAW	300.27	300.35 (0.03)	300.86 (0.20)	59.89	59.81 (−0.14)	59.30 (−0.98)
TRO	244.10	244.25 (0.06)	243.76 (−0.14)	116.06	115.91 (−0.13)	116.40 (0.30)
USS	272.56	272.68 (0.05)	273.03 (0.17)	87.60	87.48 (−0.14)	87.13 (−0.54)

is taken to be 50 cm^{-1}. The solar irradiances at TOA are taken from Thekaekara (1973). Again, 145 quadrature points were employed to perform the integration in g space. Finally, we may use CKD to calculate solar fluxes and heating rates in nonscattering atmospheres. The other quantity of interest is the total absorbed flux within the atmosphere, which is defined by $F_a = F^{\downarrow}(\text{TOA}) - F^{\downarrow}(0)$.

Comparisons of the LBL and CKD methods for the calculation of downward solar fluxes at surface and total atmospheric absorption due to H_2O in the spectral region 2500–14 500 cm^{-1} are given in Table 3 using a solar zenith angle of 60°. In Table 4, the results are presented for a number of solar zenith angles using the midlatitude summer atmosphere. As in the case of thermal infrared radiation, the correlated assumptions underestimate total atmospheric absorption. Since absorption is the only radiative process that is considered in the solar region, CKD overestimates the downward solar flux at the surface. Overall, results from CKD yield relative accuracies within ~0.05% and 0.14% for $F^{\downarrow}(0)$ and F_a, respectively.

The heating rate profiles produced by LBL and the corresponding error profiles associated with CKD are shown in Fig. 7 for four different atmospheres using a solar zenith angle of 60°. In Fig. 8, the results are presented for a number of solar zenith angles using the midlatitude summer atmosphere. Figures 7 and 8 illustrate that the results from CKD agree with those from LBL within ~0.01 K day^{-1}.

The optimum number of g values that can achieve accuracy within about 1% for H_2O lines in each spectral band is shown in Table 2. Tables 3 and 4 show that $F^{\downarrow}(0)$ and F_a can yield relative accuracies better than 0.3% and 1%, respectively, when the number of quadrature points is reduced to 10 (Table 2). Errors in the

TABLE 4. Same as Table 3 except for three different solar zenith angles, using the midlatitude summer atmosphere.

	$F^{\downarrow}(0)$			F_a		
	LBL	CKD	CKDA	LBL	CKD	CKDA
30°	462.84	463.05	463.48	160.96	160.75	160.32
		(0.04)	(0.14)		(−0.13)	(−0.40)
60°	253.29	253.43	253.30	106.87	106.73	106.86
		(0.06)	(0.00)		(−0.13)	(−0.01)
75°	121.78	121.86	121.42	64.66	64.57	65.02
		(0.07)	(−0.29)		(−0.13)	(0.56)

heating rate due to H_2O in the spectral region 2500–14 500 cm^{-1} are less than 0.05 K day^{-1}, as shown in Figs. 9a and 9b, in which the heating rate errors are presented for four atmospheric profiles for a solar zenith angle of 60° and three solar zenith angles using the midlatitude summer atmosphere.

5. Treatment of the overlap of absorption bands

Wang and Ryan (1983) have illustrated the importance of treating overlap absorption in radiative transfer calculations and climate studies. Since computational speed is essential to radiative transfer modeling, overlap absorption by several different gases becomes an important theoretical and practical problem in CKD, especially when it is applied to scattering atmospheres. In this section, we provide two different approaches to treat overlap absorption in g space. The first approach uses the multiplication assumption.

The spectral-mean transmittance of two different gases for a given spectral interval can be expressed as

$$T_{\bar{\nu}}(1,2) = \int_{\Delta\nu} T_\nu(1) \times T_\nu(2) \frac{d\nu}{\Delta\nu}, \tag{5.1}$$

where the numbers 1 and 2 denote two different gases. If $T_\nu(1)$ and $T_\nu(2)$ are uncorrelated, we may write

$$T_{\bar{\nu}}(1,2) = \int_{\Delta\nu} T_\nu(1) \frac{d\nu}{\Delta\nu} \times \int_{\Delta\nu} T_\nu(2) \frac{d\nu}{\Delta\nu} = T_{\bar{\nu}}(1) \times T_{\bar{\nu}}(2). \tag{5.2}$$

Using Eq. (5.2), we may express the spectral-mean transmittance in g space in the form

$$\begin{aligned} T_{\bar{\nu}}(1,2) &= \int_0^1 \exp\left(-\int_{z_1}^{z_2} k_1\rho_1 dz\right) dg_1 \\ &\times \int_0^1 \exp\left(-\int_{z_1}^{z_2} k_2\rho_2 dz\right) dg_2 \\ &= \int_0^1 \int_0^1 \exp\left[-\int_{z_1}^{z_2} (k_1\rho_1 + k_2\rho_2) dz\right] dg_1 dg_2 \\ &\approx \sum_{m=1}^{M} \sum_{n=1}^{N} \exp(-\tau_{mn}) \Delta g_{1m} \Delta g_{2n}, \end{aligned} \tag{5.3}$$

where ρ_1 and ρ_2 are densities for gases 1 and 2, M and N denote the number of g values for the two gases, and the optical depth is defined by

$$\tau_{mn} = \int_{z_1}^{z_2} (k_{1m}\rho_1 + k_{2n}\rho_2) dz. \tag{5.4}$$

Equations (5.3) and (5.4) allow us to use the equivalent k functions of the individual gases to resolve the overlap problem.

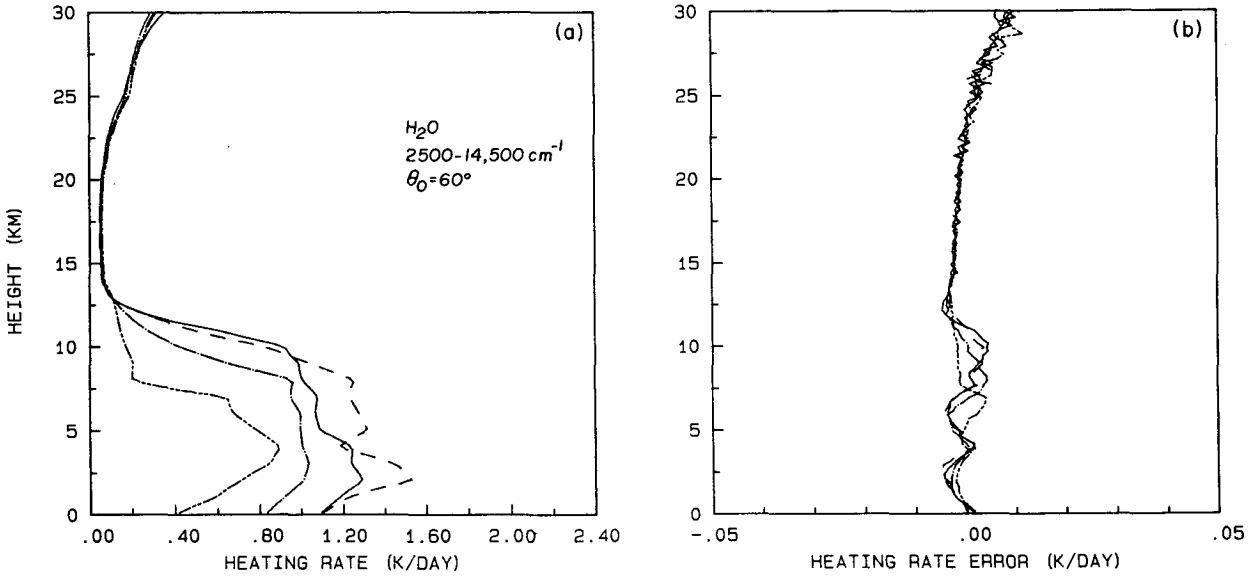

FIG. 7. (a) Heating-rate profiles computed from LBL and (b) the error profiles produced by CKD for the H_2O bands in the solar spectral region 2500–14 500 cm^{-1} for the midlatitude summer (solid), subarctic winter (double dot-dashed), tropical (dashed), and U.S. Standard (dot-dashed) atmospheres. The solar zenith angle used is 60°.

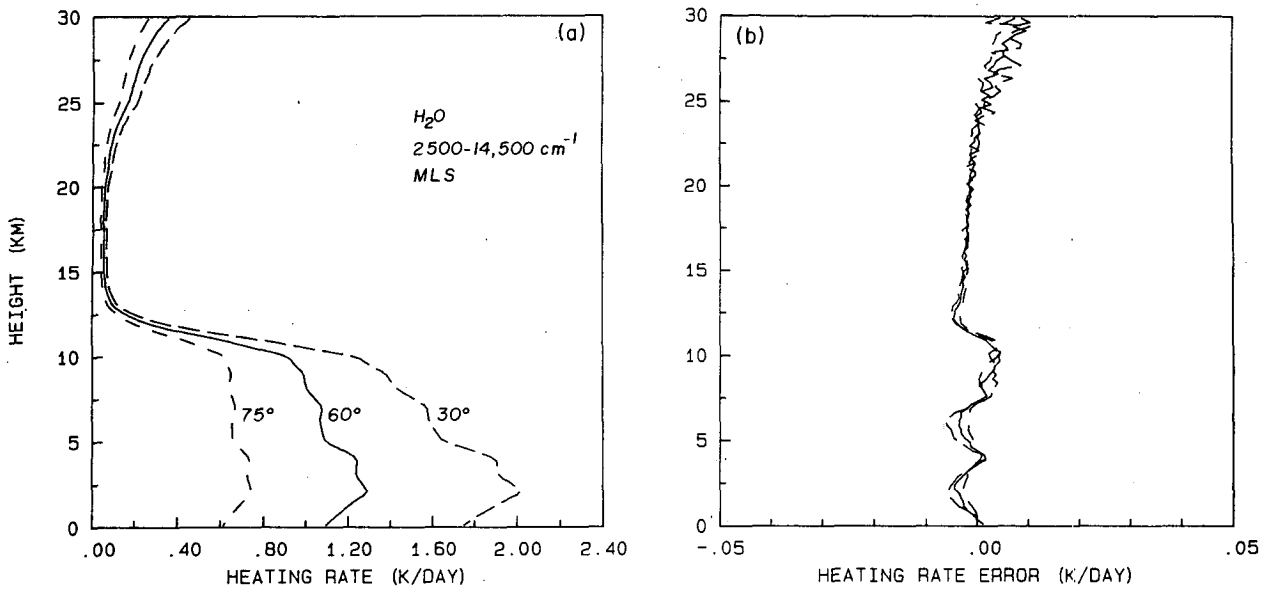

FIG. 8. Same as Fig. 7, except for three solar zenith angles of 30° (long dashed), 60° (solid), and 75° (short dashed) using the midlatitude summer atmosphere.

Ackerman (1979) carried out LBL calculations to investigate the CO_2–H_2O overlap problem. Computations were made based on Eqs. (5.1) and (5.2) using a 5-cm^{-1} spectral width. A comparison of the multiplicative transmittance with the combined transmittance shows differences of less than 1% in the test region. This suggests that the error introduced by multiplying the two transmittances is not likely to be of significance for a 5-cm^{-1} spectral width. However, it is not practical to employ this small spectral interval in a radiation scheme because of the large computational efforts involved. In the present study, the bandwidth in which overlap occurs ranges from 120 to 180 cm^{-1} (Table 2). For these bandwidths, the accuracy of using Eq. (5.3) in flux and heating rate calculations must be examined. As in section 4, we use 145 quadrature

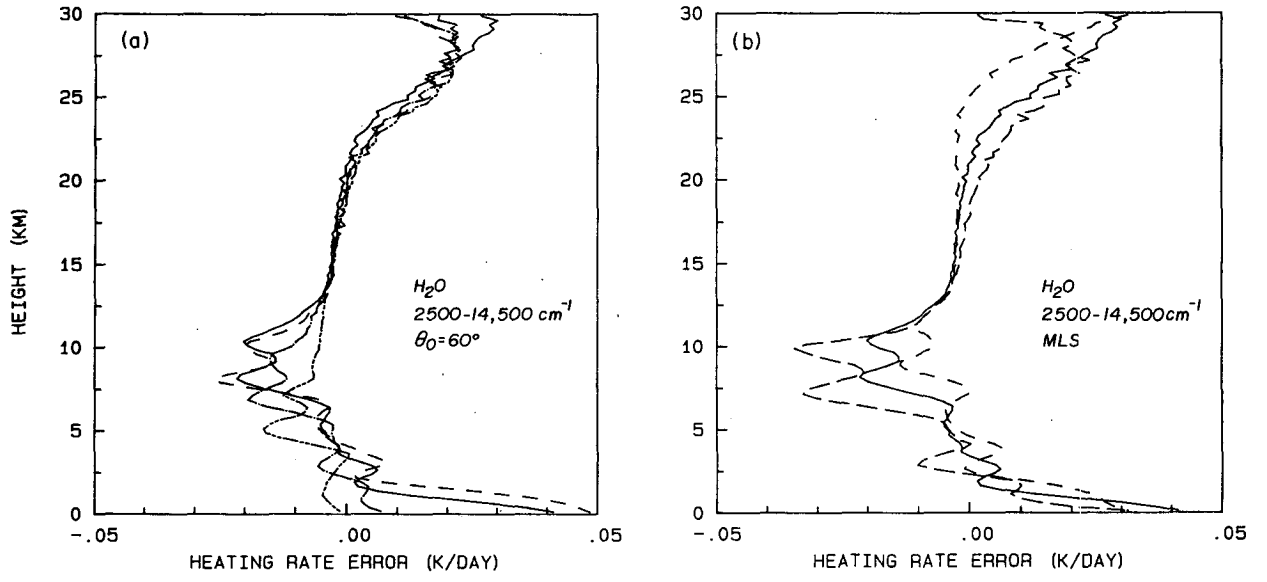

FIG. 9. (a) Heating rate error profiles produced by CKDA for the H_2O bands in the spectral region 2500–14 500 cm^{-1} for the midlatitude summer (solid), subarctic winter (double dot-dashed), tropical (dashed), and *U.S. Standard* (dot dashed) atmospheres. The solar zenith angle used is 60°. (b) Same as in (a), except for three solar zenith angles, 30° (long dashed), 60° (solid), and 75° (short dashed) using the midlatitude summer atmosphere.

points to perform g integration. Unlike the case of individual gases, errors in CKD results are also caused by overlap treatment.

Table 5 shows a comparison of LBL and CKD calculations for fluxes due to overlap absorption bands using the midlatitude summer atmosphere. In LBL calculations, the spectral-mean transmittance is computed from Eq. (5.1). The 15-μm region (540–800 cm^{-1}), where CO_2 and H_2O lines overlap significantly, represents an important example of overlap absorption. As shown in Table 5, the relative errors in $F^{\downarrow}(0)$ and $F^{\uparrow}(TOA)$ are about 1.2%. By comparing the results in Table 5 with those in Table 1, we find that the multiplication approximation for a 130 cm^{-1} spectral width involving H_2O and CO_2 in the 540–800 cm^{-1} region produces a 1% relative error in fluxes. Another example that can be used to test the accuracy of CKD for overlap gases is the 7–8-μm region (1100–1400 cm^{-1}) where CH_4, N_2O, and H_2O lines overlap. When we use the multiplication property over a 150 cm^{-1} width, the relative errors for CKD in fluxes are also ~1% (Table 5), which is largely due to the multiplication approximation. The fluxes due to H_2O (with continuum) + CO_2 + O_3 + CH_4 + N_2O in the spectral region 0–2200 cm^{-1} are also calculated by CKD using the multiplication approximation to account for overlap absorption. We include continuum absorption in the 280 to 1250 cm^{-1} spectral region (Roberts et al. 1976). Table 5 shows that the errors produced by CKD are 0.07% (0.25 W m^{-2}) and 0.46% (1.3 W m^{-2}) for $F^{\downarrow}(0)$ and $F^{\uparrow}(TOA)$, respectively.

Comparisons of the heating rate profiles due to overlap absorption bands are shown in Fig. 10 using midlatitude summer atmosphere. For CO_2 and H_2O (lines only) in the spectral region 540–800 cm^{-1} (Fig. 10a and 10b), the maximum difference of ~0.15 K day^{-1} in heating rates occurs at ~50 km, which is caused by the correlated assumptions. The agreement below 30 km is excellent; errors are within 0.05 K day^{-1} with respect to LBL results. These errors are largely due to the multiplication approximation. For CH_4 + N_2O + H_2O (lines only), errors in the heating rate are less than 0.02 K day^{-1}, as shown in Fig. 10d. For all constituents (Fig. 10e and 10f), errors in the heating rates near the surface are ~0.08 K day^{-1}; this is primarily caused by the multiplication approximation. The maximum difference of ~0.25 K day^{-1} that occurs at ~55 km is caused by the correlated assumptions.

TABLE 5. Comparison of the line-by-line and correlated k-distribution methods for radiative fluxes (W m^{-2}) at the top and surface due to overlap absorption bands using the midlatitude summer atmosphere. The percentage error is in parentheses.

$F^{\downarrow}$ (0)		$F^{\uparrow}$ (TOA)	
LBL	CKD	LBL	CKD
H_2O (lines only) + CO_2 540–800 cm^{-1}			
97.45	96.27 (−1.2)	68.67	69.53 (1.3)
H_2O (lines only) + CH_4 + N_2O 1100–1400 cm^{-1}			
28.61	28.39 (−0.77)	34.53	35.05 (1.5)
H_2O (with continuum) + CO_2 + O_3 + CH_4 + N_2O 0–2200 cm^{-1}			
348.16	348.42 (0.07)	283.87	285.17 (0.46)

In view of the preceding comparisons, we conclude that using Eq. (5.3) for overlap gases over a spectral interval of ~150 cm^{-1} can achieve excellent accuracy in flux and heating rate calculations. Although we may improve the accuracy by reducing $\Delta\nu$, computational effort must be increased.

Based on Eqs. (5.3) and (5.4), we may use CKD to obtain overlap absorption optical depth for incorporation in scattering calculations. However, we must perform $M \times N$ spectral calculations for each vertical column in order to obtain fluxes and heating rates in a spectral interval where two gases overlap. If the optimum number of g shown in Table 2 is used in the calculations, we find that the application of the multiplication approximation for overlap absorption would introduce additional computational efforts in the spectral region 540–800 cm^{-1} where CO_2 and H_2O lines overlap. For this overlap, we must carry out 82 ($5 \times 10 + 4 \times 8$) computations. To economize the computational efforts, we have developed another approach to resolve the overlap problem in the context of CKD.

For $CO_2(1)$ and $H_2O(2)$, the optical depth for a given wavenumber ν can be expressed as

$$\tau_1(\nu) = q_c \int k_1(\nu, p, T)\rho_a dz,$$

$$\tau_2(\nu) = \int k_2(\nu, p, T) q \rho_a dz, \qquad (5.5)$$

where q_c and q are the mixing ratios for CO_2 and H_2O, respectively, and ρ_a is the air density.

Using the multiplication property, which is exact for a given wavenumber, the total optical depth may be written as

$$\tau(\nu) = \tau_1(\nu) + \tau_2(\nu) = q_c \int k(\nu, p, T, q)\rho_a dz, \qquad (5.6)$$

where we define

$$k(\nu, p, T, q) = k_1(\nu, p, T) + \frac{q}{q_c} k_2(\nu, p, T). \qquad (5.7)$$

The term k may be considered as the absorption coefficient for a single-mixture gas.

As in the case of individual gases, we may define a k-distribution function, $h(k, p, T, q)$, for given p, T,

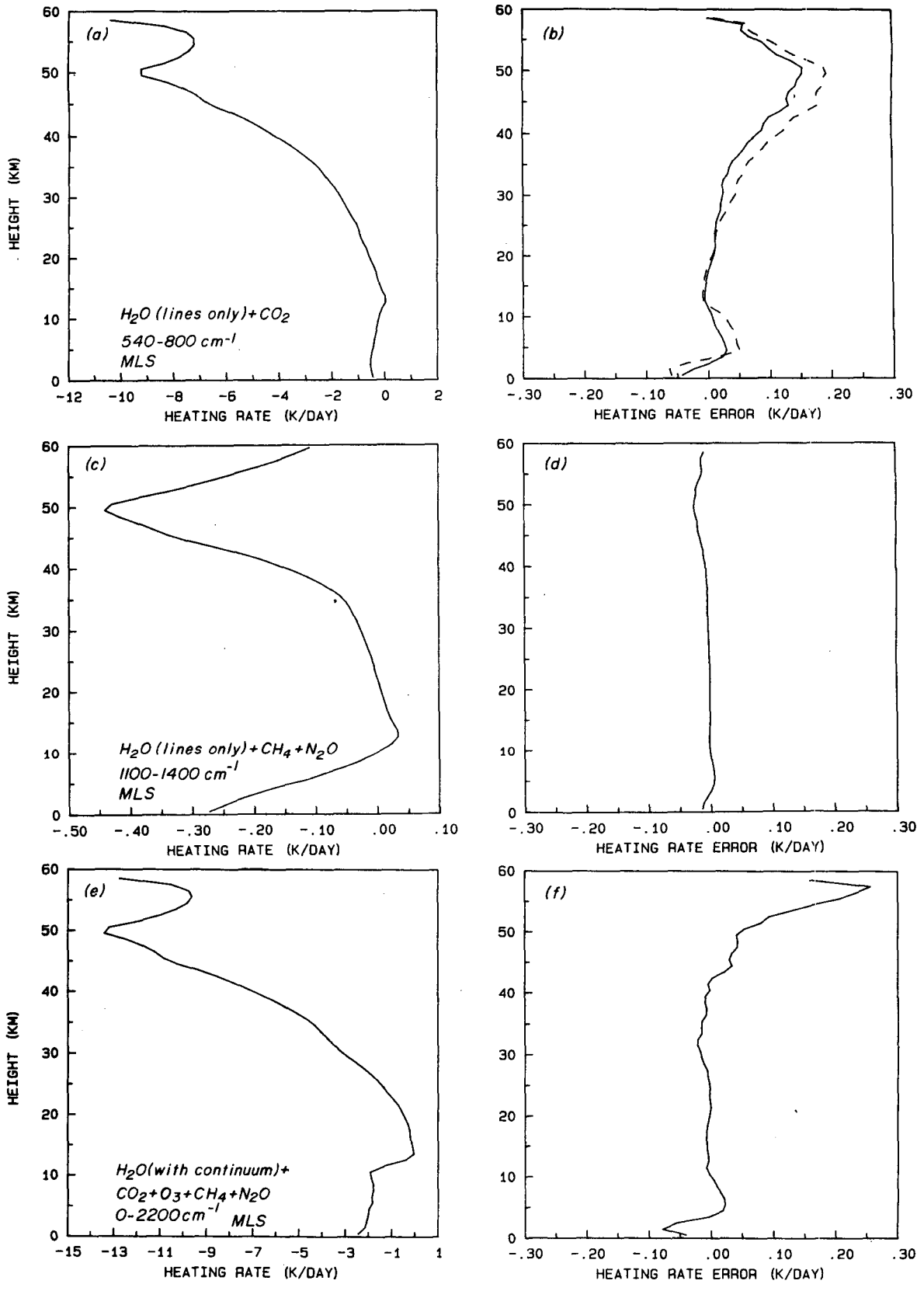

FIG. 10. Heating rate profiles computed from LBL and the error profiles produced by CKD for the overlap absorption bands in the midlatitude summer atmosphere. (a) and (b) are for H_2O (lines only) + CO_2; (c) and (d) are for H_2O (lines only) + CH_4 + N_2O; and (e) and (f) are for H_2O (with continuum) + CO_2 + O_3 + CH_4 + N_2O. The dashed line in Fig. 10b is the error profile produced by CKD for a single-mixture gas consisting of H_2O and CO_2.

and q from $k(\nu, p, T, q)$. Subsequently, the cumulative probability function can be expressed in the form

$$g(k, p, T, q) = \int_0^k h(k, p, T, q)dk. \quad (5.8)$$

Since $g(k, p, T, q)$ is a monotonic function of k for given p, T, and q, we may obtain the inverse of this function, $k(g, p, T, q)$.

The CKD for a single-mixture gas requires the same correlated assumptions as those for an individual gas, except that one additional variable, q, is needed. Under the correlated assumptions, g can replace ν as an independent variable from one layer (p_i, T_i, q_i) to another layer (p_j, T_j, q_j). To facilitate the computation of $k(g, p, T, q)$, we have developed the following parameterization:

$$k(g, p, T, q) = \exp[\sum_{n=0}^{2} A_n(g, p)(T - 250)^n] + q \exp[\sum_{n=0}^{2} B_n(g, p)(T - 250)^n], \quad (5.9)$$

where the coefficients A_n and B_n ($n = 0, 1, 2$) were determined by three temperatures and two H_2O mixing ratios for 19 pressures and 145 g. The equivalent k function for other pressures can be interpolated linearly in the pressure coordinate. Because of the additional blurring of the correlated assumptions due to the variability of the water vapor mixing ratio, we anticipate that CKD would produce more errors. Errors in the heating rate are less than 0.06 and 0.2 K day^{-1} below and above 30 km, respectively (Fig. 10b, dashed line). Errors in the fluxes are ~1%. Compared with CKD results, the optimum number of g values for each band that would produce 1% accuracy in fluxes and heating rates may be determined. We find that the optimum numbers are 12 and 10 for the 540–670 and 670–800 cm^{-1} spectral bands, respectively. Thus, the second approach, which is similar to the first in accuracy, reduces the computational efforts by a factor of 4.

In summary, the equivalent k function has been obtained for a single-mixture gas to handle the overlap absorption of CO_2 and H_2O in the 540–800 cm^{-1} spectral region. This new procedure will greatly enhance computational efficiency. In this procedure, the assumption that the two absorption spectra are uncorrelated is not required. Finally, by using the optimum number of g values, we obtain 67 infrared subintervals for all principal gases, including overlaps. Compared with LBL results, the errors in the heating rate are within ~0.08 K day^{-1} (~4%) below ~30 km. For $F^{\downarrow}(0)$ and $F^{\uparrow}(\text{TOA})$, the errors are less than 0.15% (0.52 W m^{-2}) and 0.43% (1.22 W m^{-2}), respectively.

6. Conclusions

We have examined the correlated k-distribution method for the calculation of radiative transfer in nonhomogeneous atmospheres in terms of the physical and mathematical conditions under which this method is correct. We show that two correlated conditions are necessary and sufficient for the exact transformation of the wavenumber integration to an integration over g space. These conditions involve the use of a reference condition to define the absorption coefficient and an assumption concerning the ordering of the absorption coefficient. The correlated conditions are correct in the context of a single line, periodic lines, and strong- and weak-line limits. For realistic absorption spectrum, we present the deviation of the correlated assumptions due to the pressure and temperature differences. These assumptions are best for adjacent levels but produce increased blurring for levels further apart.

In terms of numerical calculations, we compute the g function directly from the LBL absorption coefficient spectrum. We have developed efficient and accurate parameterizations for the calculation of the equivalent k function for arbitrary pressures and temperatures. It suffices to precompute this function at three temperatures and 19 pressures (or 11 pressures for solar spectrum).

We have used a variety of atmospheric profiles and spectral intervals containing principal absorbers to investigate the effects of the correlated assumptions on the computations of fluxes and heating rates. In the thermal infrared, errors in fluxes for gases other than O_3 are less than 0.2%. For O_3, flux errors are ~2%. Errors in heating rates are less than 0.01 K day^{-1} below ~30 km for all gases. Above this height, errors are less than 0.24 and 0.1 K day^{-1} for H_2O and $CO_2(O_3)$, respectively. In the solar region, errors in fluxes are less than 0.05%, while errors in heating rates are less than 0.01 K day^{-1}. Numerical results reveal that the CKD approach underestimates and overestimates the downward surface flux in the thermal infrared and solar regions, respectively. These systematic errors are produced by the correlated assumptions.

We have explored the optimum number of g values that will yield acceptable accuracy in the calculation of fluxes and heating rates. Based on numerical experimentation, we find that the number of g values ranging from 1 (for weak absorption bands) to ~10 (for strong absorption bands) are usually sufficient for atmospheric radiative transfer calculations. To facilitate the computations involving overlap bands, we have developed an approach based on the concept of the correlated conditions in which the water vapor mixing ratio is introduced as an additional independent variable. This approach allows us to significantly reduce the number of g values for the H_2O–CO_2 overlap and, at the same time, maintain the accuracy requirement.

As pointed out in section 2, the CKD approach differs from the traditional approach that employs band models and scaling approximations to separate wavenumber and height integrations. In CKD, the height integration can readily be performed once the k values are determined. The accuracy of this approach in flux

and heating-rate calculations has been shown to be superior to the conventional scaling approaches. Acceptable accuracy can be achieved by nominal computer time (e.g., 67 calculations for the entire infrared spectrum containing all principal absorbing gases). Moreover, the equivalent k function for various gases can be directly incorporated in the multiple-scattering program that includes the scattering and absorption contributions of cloud and aerosol particles.

Acknowledgments. The research work contained herein has been supported by NASA Grant NAG5-1050, AFOSR Grant 91-0039, and, in part, by NSF Grant 90-24217. We thank Dr. M. D. Chou for providing us with his line-by-line program and for his advice on our research program.

REFERENCES

Ackerman, T. P., 1979: On the effect of CO_2 on atmospheric heating rates. *Tellus,* **31,** 115–123.

Ambartzumian, V., 1936: The effect of the absorption lines on the radiative equilibrium of the outer layers of the stars. *Publ. Obs. Astron. Univ. Leningrad,* **6,** 7–18.

Arking, A., and K. Grossman, 1972: The influence of line shape and band structure on temperatures in planetary atmospheres. *J. Atmos. Sci.,* **29,** 937–949.

Chou, M.-D., and A. Arking, 1980: Computation of infrared cooling rates in the water vapor bands. *J. Atmos. Sci.,* **37,** 855–867.

——, and L. Kouvaris, 1986: Monochromatic calculations of atmospheric radiative transfer due to molecular line absorption. *J. Geophys. Res.,* **91,** 4047–4055.

——, and ——, 1991: Calculation of transmission functions in the infrared CO_2 and O_3 bands. *J. Geophys. Res.,* **96,** 9003–9012.

Domoto, G. A., 1974: Frequency integration for radiative transfer problems involving homogeneous non-grey cases: The inverse transmission function. *J. Quant. Spectrosc. Radiat. Transfer,* **14,** 935–942.

Elsasser, W. M., 1938: Mean absorption and equivalent absorption coefficients of a band spectrum. *Phys. Rev.,* **54,** 126–129.

Fu, Q., 1991: Parameterization of radiative processes in vertically nonhomogeneous multiple scattering atmospheres. Ph.D. dissertation, University of Utah, 259 pp.

Goody, R. M., 1964: The transmission of radiation through an inhomogeneous atmosphere. *J. Atmos. Sci.,* **21,** 575–581.

——, and Y.-L. Yung, 1989: *Atmospheric Radiation: Theoretical Basis.* Oxford University Press, 519 pp.

——, R. West, L. Chen, and D. Crisp, 1989: The correlated-k method for radiation calculation in nonhomogeneous atmospheres. *J. Quant. Spectrosc. Radiat. Transfer,* **42,** 539–550.

Kratz, D. P., and R. D. Cess, 1988: Infrared radiation models for atmospheric ozone. *J. Geophys. Res.,* **93,** 7047–7054.

Lacis, A., and V. Oinas, 1991: A description of the correlated k-distribution method for modeling nongray gaseous absorption, thermal emission, and multiple scattering in vertically inhomogeneous atmospheres. *J. Geophys. Res.,* **96,** 9027–9063.

——, W. C. Wang, and J. Hansen, 1979: Correlated k-distribution method for radiative transfer in climate models: Application to effect of cirrus clouds on climate. NASA Conf. Publ. 2076, 309–314.

Liou, K.-N., 1980: *An Introduction to Atmospheric Radiation.* Academic Press, 392 pp.

——, Q. Fu, and T. P. Ackerman, 1988: A simple formulation of the delta-four-stream approximation for radiative transfer parameterization. *J. Atmos. Sci.,* **45,** 1940–1947.

McClatchey, R. A., R. W. Fenn, J. E. A. Selby, F. E. Volz, and J. S. Garing, 1971: Optical properties of the atmosphere. Rep. AFCRL-71-0279, 85 pp., Air Force Cambridge Res. Lab., Bedford, MA.

——, W. S. Benedict, S. A. Clough, D. E. Burch, R. F. Calfee, K. Fox, C. S. Rothman, and J. S. Garing, 1973: AFCRL atmospheric absorption line parameters compilation. Environ. Res. Pap. 434, Air Force Cambridge Res. Lab., Hanscom AFB, Bedford, MA.

Roberts, R. E., J. E. A. Selby, and L. M. Biberman, 1976: Infrared continuum absorption by atmospheric water vapor in the 8–12 μm window. *Appl. Opt.,* **15,** 2085–2090.

Rothman, L. S., R. R. Gamache, A. Barbe, A. Goldman, J. R. Gillis, L. R. Brown, R. A. Toth, J.-M. Flaud, and C. Camy-Peyret, 1983: AFGL atmospheric line parameters compilation: 1982 edition. *Appl. Opt.,* **22,** 2247–2256.

——, ——, A. Goldman, L. R. Brown, R. A. Toth, H. M. Pickett, R. L. Poynter, J.-M. Flaud, C. Camy-Peyret, A. Barbe, N. Husson, C. P. Rinsland, and M. A. H. Smith, 1986: The HITRAN database: 1986 edition. *Appl. Opt.,* **26,** 4058–4097.

Stephens, G. L., 1984: The parameterization of radiation for numerical weather prediction and climate models. *Mon. Wea. Rev.,* **112,** 826–867.

Thekaekara, M. P., 1973: Solar energy outside the earth's atmosphere. *Sol. Energy,* **14,** 109–127.

Wang, W.-C., and P. B. Ryan, 1983: Overlapping effect of atmospheric H_2O, CO_2 and O_3 on the CO_2 radiative effect. *Tellus,* **35B,** 81–91.

West, R., D. Crisp, and L. Chen, 1990: Mapping transformations for broadband atmospheric radiation calculations. *J. Quant. Spectrosc. Radiat. Transfer,* **43,** 191–199.

Whittacker, E. T., and G. N. Watson, 1940: *Modern Analysis.* Cambridge University Press, 595 pp.

Wu, M. L., 1980: The exchange of infrared radiative energy in the troposphere. *J. Geophys. Res.,* **85,** 4084–4090.

Yamamoto, G., M. Aida, and S. Yamamoto, 1972: Improved Curtis–Godson approximation in a non-homogeneous atmosphere. *J. Atmos. Sci.,* **29,** 1150–1155.